Mitochondrial Networks in Cardiac Myocytes Reveal Dynamic Coupling Behavior

Felix T Kurz, MD

Thomas Derungs, MS

Miguel A Aon, PhD

Brian O'Rourke, PhD

Antonis A Armoundas, PhD

Experimental Methods

Isolated Myocyte Preparation

All experiments have been conducted on freshly isolated adult guinea pig ventricular myocytes according to previously described protocols (1-3) and in accordance with Guide for the Care and Use of Laboratory Animals (NIH, No. 85-23, 1996) and the Johns Hopkins Animal Care and Use Committee. Adult guinea pigs (300 g) were anesthetized with 260 mg pentobarbital and 1000 U heparin sodium (i.p.).

Hearts were excised and ventricular myocytes were enzymatic isolated as previously described (3). After isolation, myocytes were stored briefly in a high K+ solution (in mM: 120 potassium glutamate, 25 KCl, 1 MgCl2, 10 HEPES, 1 EGTA, pH 7.2 (with KOH) and either used immediately or transferred to Dulbecco's Modification of Eagle's Medium (10-013 DMEM, Mediatech, Inc. Virginia, Manassas, VA, USA) in laminin-coated petri dishes in a 95% O_2, 5% CO_2 incubator at 37°C for 1-2 h before imaging. Experimental recordings started after exchange of the DMEM with Tyrode's solution containing (in mM): 140 NaCl, 5 KCl, 1 $MgCl_2$, 10 HEPES, 1 $CaCl_2$, pH 7.4 (adjusted with NaOH), supplemented with 10 mM of glucose, or β-hydroxybutyrate, or lactate or pyruvate.

Whole Heart Preparation

Excised hearts were retrogradely perfused with an oxygenated (100% O_2) modified Tyrode's solution (138 mM NaCl, 4 mM KCl, 0.5 mM $CaCl_2$, 1 mM $MgCl_2$, 0.33 mM NaH_2PO_4, 10 mM glucose, 10 mM HEPES pH 7.4 containing 20mM butanedione monoxime (BDM) to suppress contraction (4). A custom-built chamber was used to minimize pulsatile motion artifacts and imaging focused on epicardial regions located near (within 5 mm) the left anterior descending coronary artery (5).

Imaging Studies

The cationic potentiometric fluorescent dye tetramethylrhodamine ethyl ester (TMRE) was used to monitor the mitochondrial inner membrane potential $\Delta\Psi_m$ and images were recorded with a two-photon laser-scanning microscope (Bio-Rad MRC-1024MP, Hercules, CA, USA) using excitation at 740 nm (Tsunami Ti:Sa laser, Spectra-Physics, Santa Clara, CA, USA) and emission at 605±45nm.

Selection and processing of TMRE fluorescence from individual mitochondria in isolated cardiac myocytes

TMRE signals from individual mitochondria were analyzed in stacks of recorded frames of isolated myocytes by manually applying a grid template to the myocytes. Stack images were time-averaged using Adobe Photoshop v7.0 according to previously described methods (6) (Figure 1B in main text). Briefly, time-dependent mesh identifiers appplied to each myocyte allowed the identification of individual mitochondria, while correction for myocyte movement was accomplished with ImageJ (v.1.40g).

Selection of wavelet parameters, cut-off frequencies, normalization of mitochondrial TMRE signals and determination of maximal wavelet power frequencies were carried out according to the modus operandi in (6, 7). Morlet wavelets were used for each mitochondrion's TMRE signal with spacing between scales set to $dj = 0.1$.The smallest wavelet scale was set to $s_0 = 4dt$ since this scale size represents the smallest possible scale that could be detected during one oscillatory cycle. With the total number, N, of recorded images per myocyte, the number of scales was taken as $j_1 = \log_2(N/s_0)/dj + 1$. Therefore, scales range from s_0 to $s_0 2^{(j_1-1)dj}$ and each scale has dj suboctaves. Cut-off frequencies were chosen for each myocyte according to the longest observed oscillation period, T, and therefore the minimum cut-off frequency was defined as $\nu_{\min} = 1/1.1T$. The maximum cut-off frequency was fixed at

$\nu_{max} = 1/s_0$, the highest possibly observable period. Between ν_{min} and ν_{max}, for each myocyte, power line plots with segments of 0.1 mHz were interpolated and, finally, the maximum power for each interpolated plot was used to determine the respective maximal scale frequency at each time point.

Determination of frequency cluster mitochondria as well as their size, frequency, amplitude and coherence properties was completed according to the algorithm for the selection of mitochondria belonging to a major frequency cluster as detailed in Kurz et al. (7). Frequency histograms were obtained for each myocyte at every time-point *t* and the largest peak of mitochondria with similar frequencies, i.e. mitochondria belonging to a (major) frequency cluster, was determined as the major cluster peak. Subsequently, mitochondria belonging to neighboring peaks, i.e. peaks whose amplitude was beyond 10% of the maximum peak and directly neighboring the major cluster peak, were incorporated into the cluster if their TMRE signal at *t* was correlated with at least 95% with the cluster signal (see also Figure 2A in (7)). Cross correlation was computed over a running window of size $T_w = 1.1T$. The procedure was repeated with the ensuing neighboring significant peaks until signal correlation dropped below 95%. The resulting mitochondria therefore form a group of oscillators at time *t* who have similar frequencies and whose signals are highly correlated, as previously described (7).

Selection and processing of individual mitochondrial TMRE fluorescent signal in the whole heart

Whole heart samples were scanned for de- and repolarizing mitochondria. Only myocytes showing at least one depolarization, i.e. a drop of more than 10% in TMRE fluorescence in some of their mitochondria were taken into account. Myocyte borders along sarcolemma and intercalated discs were manually applied on a pixel-by-pixel basis in Adobe Photoshop v7.0 (Figure 1A in the main text and Figure S1A). Grid templates were constructed for each selected myocyte and further spatio-temporal processing was done using wavelet analysis and major frequency cluster selection as in the case of the isolated myocyte (see above and (6, 7)).

Computational Methods

Mitochondrial Network Architecture

Identification of mitochondrial nearest neighbors was used as in (7) to determine the mitochondrial network's structural topology. To examine the network's connectivity properties,

inter-mitochondrial coupling was only considered for local nearest-neighbors (Figure 2 in main text).

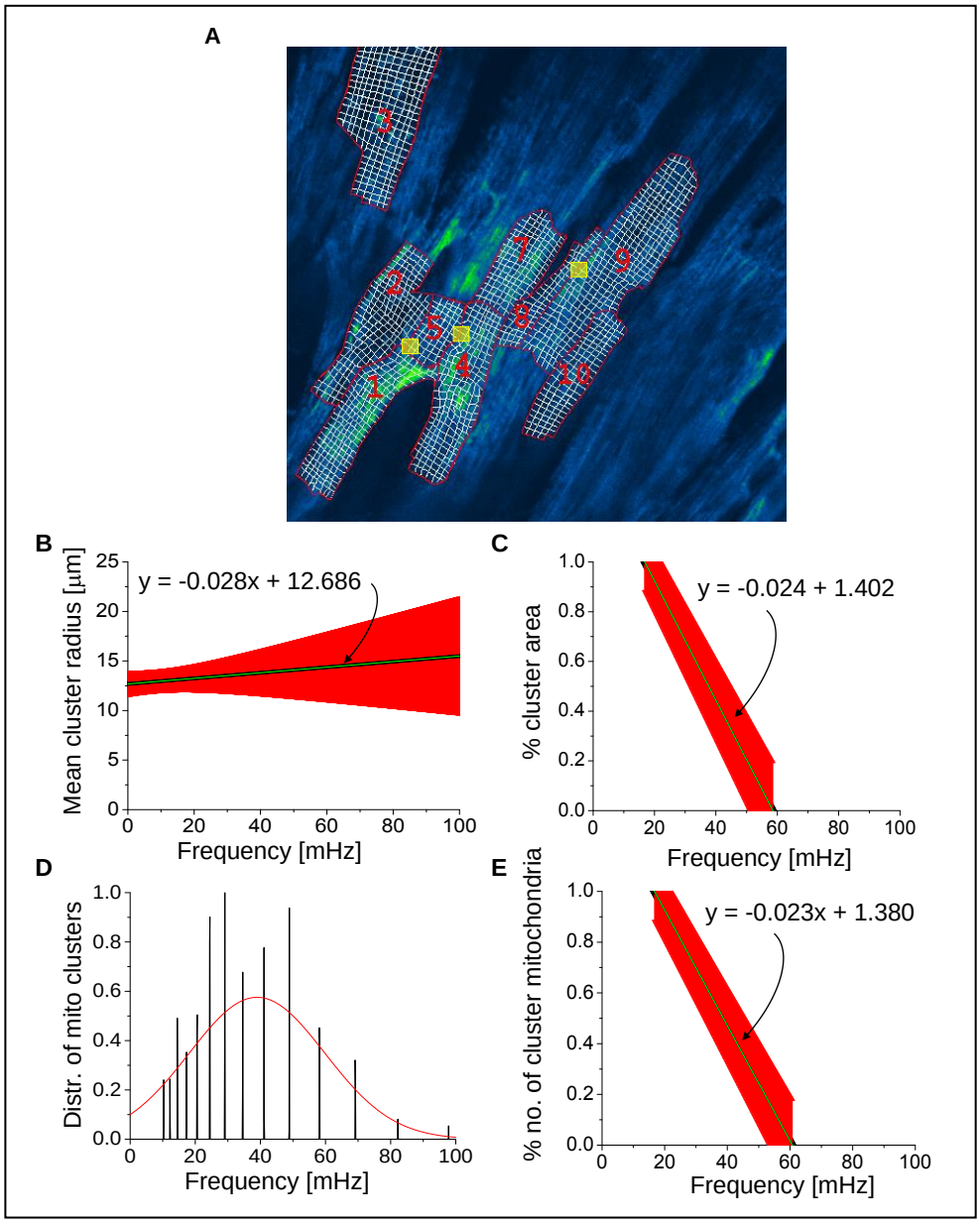

Figure S1 Two-photon image of TMRE fluorescence from intact guinea pig heart tissue (different to the one shown in Figure 3 of the main text). (A) Within the intact heart tissue, cardiac myocytes were selected according to observed depolarizations. Myocyte borders along the sarcolemma and intercalated discs, as well as the mitochondrial grids were manually applied on a pixel-by-pixel basis. Yellow boxes mark the laser flashed region of the myocytes (see main text). Mitochondrial major cluster properties of the optical slice of perfused heart tissue shown in part A (n = 9 cardiac myocytes). Displayed are the mean cluster radius versus frequency (B); the cluster area normalized by the full myocyte area versus frequency (C); the distribution of mitochondrial frequencies for all cluster mitochondria across all myocytes (D), and the cluster mitochondria count normalized by the total number of mitochondria for the major cluster versus frequency (E). A similar figure for another optical slice of the intact heart tissue can be found in the main text (Figure 1A and Figure 3).

A

$$\frac{d\varphi_m(t)}{dt} = \omega_m(t) + K_m(t)\sum_{j_i \in N} \sin\left(2\pi(\varphi_{j_i}(t) - \varphi_m(t))\right)$$

$$\frac{d\omega_m}{dt} = -\gamma(\omega_m - \mu_m) + \eta_m(t)$$

$$s(t) = \frac{1}{M}\sum_m \cos\left(\varphi_m\right)$$

B

Symbol	Description
$\varphi_m(t)$	Phase for mito *m*
$\omega_m(t)$	Intrinsic frequency for mito *m*
$\mu_m(t)$	Mean circadian frequency for mito *m*
σ_m	Frequency dispersion for mito *m*
γ	Frequency relaxation rate
$\eta_m(t)$	White noise source with variance σ_η^2
$K_m(t)$	Coupling constant for mito m
$s(t)$	Normalized intensity signal for mito *m*

Table S1 Stochastic phase model with drifting frequencies and time-dependent local mitochondrial coupling. (A) An extended Kuramoto model for the oscillator phases $\varphi_m(t)$ and frequencies $\omega_m(t)$ describes coupled circadian phase oscillators. N_m is the total number of nearest neighbors of mitochondrion *m*. The sum of the coupling term runs over all nearest neighbors j_m of mitochondrion *m*. The total luminescence signal $s(t)$ is the sum of a population of all oscillators contributing an amplitude-normalized cosine signal. *M* is the total number of mitochondrial oscillators and the sum of cosines runs over all mitochondrial oscillators. (B) Parameter listing. $K_m(t)$ represents the time-dependent local mitochondrial phase coupling constant.

Mitochondrial Wavelet Phase and Wavelet Frequency

Wavelet phases were extracted from the TMRE fluorescent signal corresponding to each mitochondrion. The wavelet transform coefficients phase at maximal wavelet power as in the frequency case. Wavelet frequencies are non-differentiable in time at points of frequency change, therefore wavelet frequencies were monitored as dynamical wavelet phase updates with the value of the actual wavelet frequency as starting point. The resulting updated wavelet

frequency was median filtered to correct for frequency changes at the turning point of phase cycles.

Ornstein-Uhlenbeck Processes

Within the stochastic coupling model of the mitochondrial network, mitochondrial intrinsic frequencies are modeled as frequencies that drift in time towards the respective measured mitochondrial frequency, i.e. the mitochondrial wavelet frequency. This accounts for dynamical changes in mitochondrial frequency and can be accomplished via Ornstein-Uhlenbeck processes that are described by the stochastic differential equation (8-10) of the form:

$$\frac{d\omega_m}{dt} = -\gamma(\omega_m - \mu_m) + \eta_m(t)$$

where μ_m represents the mean frequency towards which the intrinsic mitochondrial frequency is drifting, η_m is a Gaussian white noise source with variance $\sigma_\eta^2 = 2\gamma\sigma_m^2$, γ represents the decay rate, and σ_m^2 the amplitude of mitochondrial frequency fluctuations (9, 11). The mean frequency μ_m was chosen as the time-dependent wavelet frequency of the *m*-th mitochondrion whereas the free constant γ was assumed to be identical for each mitochondrion in the network. The frequency fluctuation amplitude measure, σ_m, for each mitochondrion was taken as the standard variation of the measured mitochondrial wavelet frequency (see Table S1).

Discrete dynamical updates were performed to calculate the mitochondrial intrinsic frequencies (12):

$$\omega_m(t+dt) = \omega_m(t)e^{-\gamma dt} + \mu_m(t)(1-e^{-\gamma dt}) + \sqrt{1-e^{-2\gamma dt}}\,\zeta \qquad (1)$$

where ζ is a random number drawn from a Gaussian distribution with zero mean and variance $\langle\zeta\rangle = \sigma_m^2$. In this step-by-step update process, *dt* represents the sampling period of the measurements of the respective myocytes. Initially, $\omega_m(0)$ was taken from a Gaussian with mean $\mu_m(dt)$ and variance σ_m^2.

Local Order Parameter Selection

Local mitochondrial coupling was considered to be of local mean field type, and local mean field parameters $R_m(t)$ and $\psi_m(t)$ corresponding to mitochondrion m are defined as

$$R_m(t)e^{2i\pi\psi_m(t)} = \frac{1}{|L_m|}\sum_{j\in L_m} e^{2i\pi\varphi_j(t)},$$

where L_m is the set of nearest neighbors of mitochondrion *m* (c.f. (9, 11)), and $|L_m|$ the number of nearest neighbors. This corresponds to phase differential equations of the form:

$$\frac{\partial\varphi_m(t)}{\partial t} = \omega_m(t) + K_m(t)R_m(t)\sin\left(2\pi(\psi_m(t)-\varphi_m(t))\right) \quad (2)$$

for each mitochondrion m.

Update Equations and Tikhonov Regularization

Within local mean field coupling, the left hand side of Eq. 2 corresponds to the updated wavelet frequency ν_m^{WT} of mitochondrion m that provides

$$\nu_m^{WT}(t) - \omega_m(t) \approx K_m(t)R_m(t)\sin\left(2\pi(\psi_m(t)-\varphi_m(t))\right) \quad (3)$$

It is evident, that K_m can become negative for some time points t_p (if $R_m(t_p)\sin\left(2\pi(\psi_m(t_p)-\varphi_m(t_p))\right)\neq 0$). In this model, we assume the mitochondrial coupling constants to be positive. This corresponds to the interpretation of an attractive coupling interaction between the oscillators, as was also originally assumed by Kuramoto (13, 14). Therefore, update equations for ω_m were subjected to the constraint:

$$\frac{\nu_m^{WT}(t)-\omega_m(t)}{R_m(t)\sin\left(2\pi(\psi_m(t)-\varphi_m(t))\right)} > 0$$

for all time points.

In addition, solving for $K_m(t)$ proves difficult at points t_0 with

$$\lim_{t\to t_0} R_m(t)\sin\left(2\pi(\psi_m(t)-\varphi_m(t))\right) \to 0$$

If one or more of such points existed for mitochondrion m, then the Tikhonov regularization was applied (15, 16). Setting

$$\mathrm{P}_m(t) = R_m(t)\sin\left(2\pi(\psi_m(t) - \varphi_m(t))\right)$$

gives the explicit solution

$$\hat{K}_\mathrm{m} = (\mathrm{P}_m^2 + \lambda 1_T)^{-1}\mathrm{P}_m^T(\nu_\mathrm{m}^\mathrm{WT} - \omega_\mathrm{m}) \quad (4)$$

with 1_T as the unity matrix of size T (T being the recording time) and Tikhonov parameter λ (16). Optimization for λ was obtained using the Hanke-Reus algorithm (15) on the interval $[(1/100)\cdot M, 100\cdot M]$, where $M = \sqrt{\mathrm{P}\mathrm{P}_m\mathrm{P}^2}/T$ is the time-averaged value of $\mathrm{P}_m(t)$. The Tikhonov parameter λ was set to $\lambda = \frac{T}{100}\sqrt{\mathrm{P}\mathrm{P}_m\mathrm{P}^2}$ when the optimization did not converge. Each curve $K_m(t)$ was padded for $t<0$ and $t>T$ with the mirror values of $K_m(t)$ for the respective vertical mirror axes at $t=0$ and $t=T$ and the resulting curves were subsequently median filtered.

Optimization of Decay Rate Parameter γ

Maximum likelihood estimation was applied to optimize the model parameter γ within the interval [0,1] s^{-1}. This interval was chosen empirically, based on the observation that normalized errors of γ in a forward model reach a global minimum plateau for values > 0.2 s^{-1} for all myocytes (see Figures S6- S7). Basically, γ was taken along the interval in steps of 0.01 to calculate γ- dependent mitochondrial coupling constants $K_m(t,\gamma)$. All coupling constants $K_m(t,\gamma)$ were consequently averaged over Ornstein-Uhlenbeck frequencies with two different starting points $\omega_m(0)$ and two differently dynamically evolving ω_m respectively.

In the next step, the $K_m(t,\gamma)$ was introduced in equation (2) together with the local mean field parameters R_m and ψ_m and random Ornstein-Uhlenbeck frequencies ω_m to model (forward) the mitochondrial phases $\varphi_m^{FM}(t,\gamma)$. The corresponding signal

$$\frac{1}{M}\sum_m \cos\left(\varphi_m^{FM}(t,\gamma)\right),$$

(where M is the total number of mitochondria) was compared for each γ against the cosine of the phase of the overall TMRE signal of the myocyte by determining the least square error. γ-dependent error values were plotted versus γ and, if they were asymptotically approaching a fixed error value, they were exponentially fitted using an exponential function ($f(x) = a \cdot \exp(-bx) + c$). Starting from time 0 and using steps of 0.01 s^{-1}, the optimal decay rate parameter for each myocyte was chosen as the first value of γ whose error value was within 1% range of the value of the asymptotic error value. If γ did not asymptotically approach a fixed error value but displayed instead a global minimum in the error values, the optimal γ was taken at this minimum.

Coupling Constants

With optimal decay rate parameter γ the coupling constants $K_m(t)$ were evaluated for 10 different starting points $\omega_m(0)$ and 100 differently dynamically evolving Ornstein-Uhlenbeck frequencies ω_m as described above.

Frequency and Cluster-Size Relationship in the Intact Perfused Heart

The rate of change of mean cluster radius with respect to the frequency for glucose-treated myocytes, in addition to the one presented in the main text (Figures 1A and 3), was also calculated for another optical slice of perfused heart tissue (Figure S1A), to be 0.03 ± 0.01 μm/mHz. The apparent discrepancy between the negative slope shown in Figure 3A of the main text and Figure S1A, is due to the determination of the geometrical center of all cluster mitochondria for a specific time point that is computed using the average $\overline{R}$ of all distances R_i of all N cluster mitochondria to the geometrical center as $\overline{R} = \sum_{i=1}^{N} R_i / N$. Naturally, for mitochondria that are distributed closely together, the average radius is smaller than in myocytes where cluster mitochondria are far apart from each other, e.g. at opposing ends of the myocyte. This explains why a cluster with more mitochondria does not necessarily have a greater radius than one with less mitochondria. This spread of mitochondria is much pronounced in the intact perfused heart in Figure S1A than for Figure 3A in the main text. This effect also explains the different frequency ranges that are due to interpolation error (see Figure 3A in the main text).

Summary statistics of mitochondrial frequency distributions of major cluster mitochondria for all cardiac myocytes of the respective whole heart yields frequency ranges of 10.30 - 100 mHz. It is evident that the range of mitochondrial frequencies in myocytes from whole heart preparations are significantly broader than in isolated myocytes, i.e., mitochondria generally oscillate at higher frequencies in the intact perfused heart. Using Figure 3A and Figure S1B we calculated a mean cluster radius of ~11 - 17 μm.

The rate of change of % area versus frequency for cardiac myocytes was determined as -2.40 ± 0.10 % / mHz. Likewise, the % number of cluster mitochondria versus frequency gave a rate of change of -2.27 ± 0.10 % / mHz. These values are in close agreement with the ones reported in the main text.

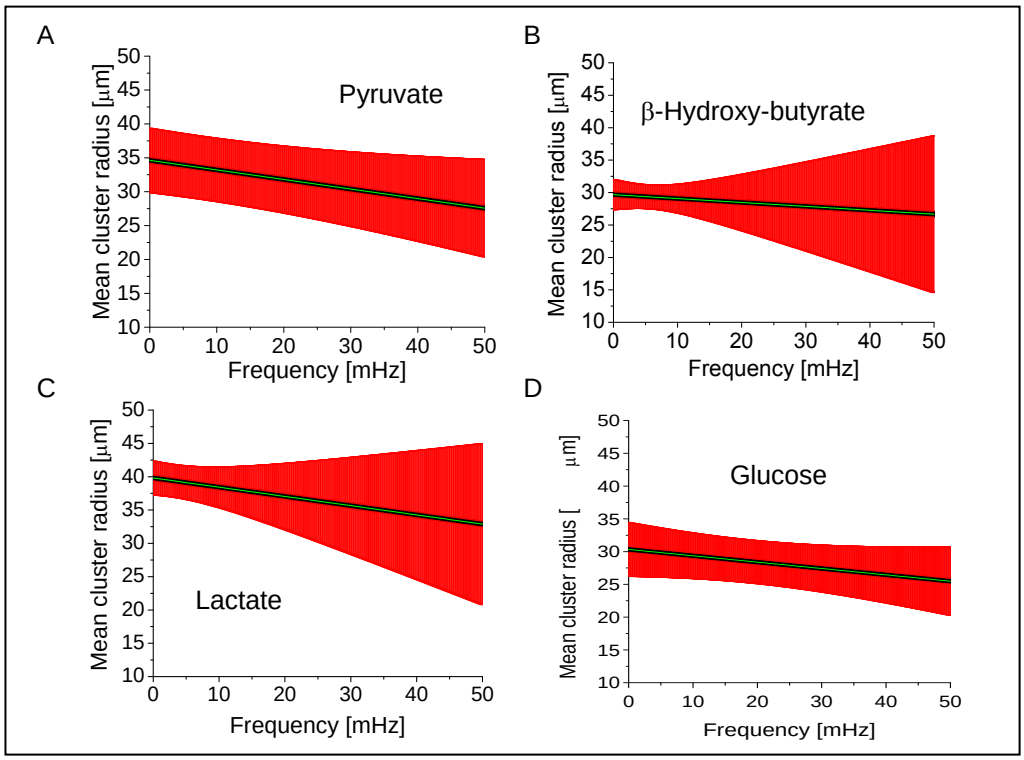

Figure S2 Mitochondrial mean cluster radius as a function of frequency. Isolated cardiac myocytes were imaged as described in Methods and perfused as described in the legend of Figure 4 with 10mM of pyruvate(A; n=10), β-hydroxybutyrate (B; n=14), lactate (C; n=7), or glucose (D; n=9).

Frequency and Cluster-Size Relationship in Isolated Myocytes

Major cluster mitochondria were determined for each myocyte treated with glucose, lactate, β-hydroxybutyrate or pyruvate. The relative number of cluster mitochondria (quotient of the number of cluster mitochondria versus the total number of mitochondria) was plotted against

the mean frequency (Figure S2). Also, measures for cluster size were compared with the mean frequency of the cluster mitochondria. Therefore, the mean cluster radius (the distance of the geometrical center of the cluster to each single cluster mitochondrion's geometrical center averaged over all cluster mitochondria) was plotted against the mean frequency of the cluster (Figure S3).

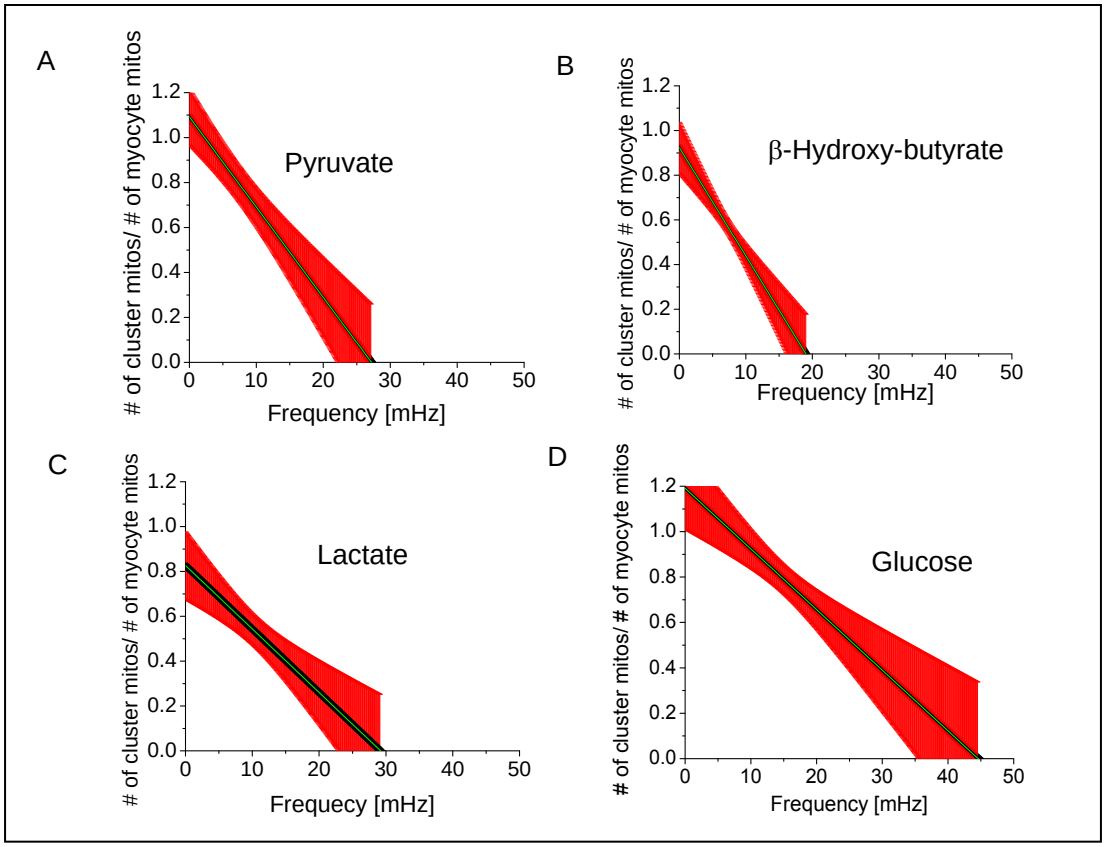

Figure S3 Mitochondrial cluster count normalized by the total number of mitochondria for the major cluster versus frequency for isolated cardiac myocytes perfused with 10mM of pyruvate (A; n=10), β-hydroxybutyrate (B; n=14), lactate (C; n=7), or glucose (D; n=9) .

From Figure S2 we obtain that the mean radius of the oscillating clusters of mitochondria for glucose-, pyruvate-, lactate- and β-hydroxybutyrate-treated myocytes is ~27 - 30 μm, ~27 - 35 μm, ~37 - 40 μm and ~29 - 30 μm, respectively. High standard errors in Figure S2 are due to topological non-contingencies of the mitochondrial major clusters, indicating a distribution of major cluster mitochondria similar to spanning clusters (7, 17, 18). In some myocytes, we have observed that with the onset of synchronized depolarizations, major frequency cluster mitochondria appear dispersed throughout the myocyte but grow more and more to be

topologically contiguous during the course of the recording. However, non-contiguous cluster mitochondria with a high degree of separately oscillating mitochondrial clusters have been observed in particular for pyruvate- or glucose-treated myocytes. The rate of change of mean radius with respect to the frequency for myocytes from the glucose-, pyruvate-, lactate- or β-hydroxybutyrate-group have been calculated to be: -0.0973 ± 0.129 μm/mHz, -0.141 ± 0.017 μm/mHz, -0.139 ± 0.018 μm/mHz and -0.060 ± 0.016 μm/mHz, respectively.

The rate of change of % number of cluster mitochondria versus frequency for glucose-, pyruvate-, lactate- or β-hydroxybutyrate-treated cardiac myocytes was determined to be -2.67 ± 1.12 % / mHz, -4.01 ± 0.07 % / mHz , -2.83 ± 0.07 % / mHz and -4.79 ± 0.07 % / mHz, respectively. This is similar to the results for % area of cluster mitochondria versus frequency as detailed in the main text.

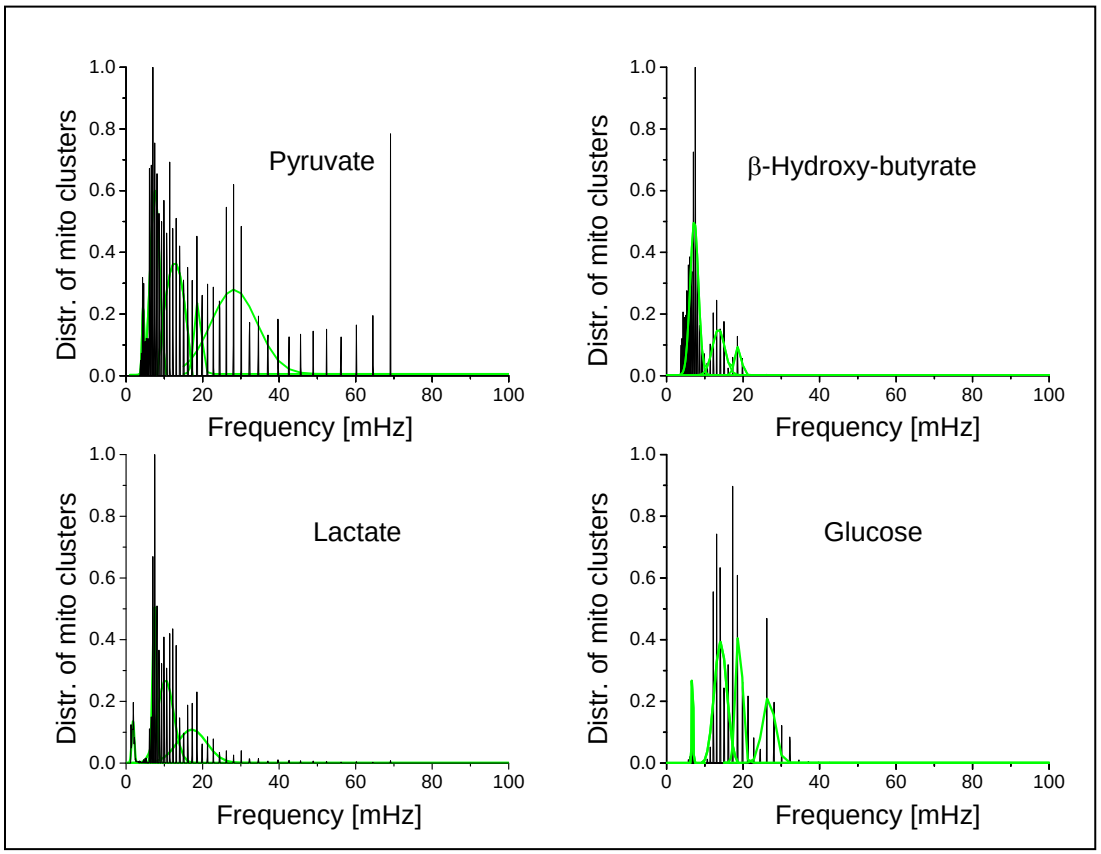

Figure S4 Distribution of mitochondrial frequencies for all cluster mitochondria across all myocytes perfused with 10mM of pyruvate (A; n=10), β-hydroxybutyrate (B; n=14), lactate (C; n=7), or glucose (D; n=9).

Distribution of mitochondrial frequencies

Frequency distributions of mitochondria belonging to the major cluster were constructed with frequency histograms across all frames (Figure S4) for each cardiac myocyte in each substrate group. Mitochondrial frequencies were counted in bins of width 0.1 mHz in the range [0-100] mHz.

To compare between myocytes within one substrate group, cluster mitochondria frequency counts in each frame were divided by the number of cluster mitochondria in that frame and amplitudes at each frequency were divided by the total number of frames. Gaussian functions were then fitted to visible peaks in the resulting histogram for each substrate group. Their position and the corresponding frequency bandwidth within the full width at half maximum (FWHM) around the mean frequency can be found in Table S2. For glucose-treated mycoytes, the overall mean frequency was found as 17.11 ± 11.88 mHz whereas, in comparison, pyruvate-treated myocytes show a more dispersed frequency distribution with a mean frequency 18.29 ± 32.20 mHz (with the lowest detectable frequency being 3.7 mHz). Myocytes from the lactate group were found to be more narrowly distributed with a mean frequency 10.14 ± 12.72 mHz (with the lowest detectable frequency being 1.3 mHz). Finally, myocytes that were perfused with β-hydroxybutyrate mostly displayed major cluster oscillations in the low frequency range 8.36 ± 8.50 mHz (with the lowest detectable frequency being 3.7 mHz).

Perfusion type / Peak #	Glucose	Pyruvate	Lactate	β-Hydroxy -Butyrate
1	6.79 ± 0.24 mHz	4.46 ± 0.63 mHz	1.822 ± 0.67 mHz	7.25 ± 2.14 mHz
2	14.12 ± 3.33 mHz	7.54 ± 2.56 mHz	7.44 ± 1.03 mHz	13.59 ± 3.18 mHz
3	18.98 ± 1.67 mHz	12.73 ± 9.23 mHz	10.31 ± 4.24 mHz	18.71 ± 1.66 mHz
4	26.71 ± 3.22 mHz	18.74 ± 1.88 mHz	17.20 ± 7.73 mHz	
5		28.21 ± 4.13 mHz		

Table S2 Multi-Peak Gaussian fit analysis for peaks in the frequency distributions of cardiac myocytes perfused with different substrates. For each peak, the mean frequency ± the FWHM are given in mHz.

Cluster Oscillation Coherence

The temporal properties of cluster mitochondria can be analyzed by investigating the average temporal coherence of the TMRE signal of a cluster mitochondrion with those of its nearest neighbors for all major cluster mitochondria. Coherence values range between 0 and 1 at each frequency representing oscillation in synchrony ("1") or asynchrony ("0"). The frequency range for each myocyte was chosen from zero to 100 mHz and coherences of each cluster mitochondrion were estimated using a running window of fixed size T_w and a fixed Fast-Fourier-Transform (FFT) of length $2^{11}dt$ (7).

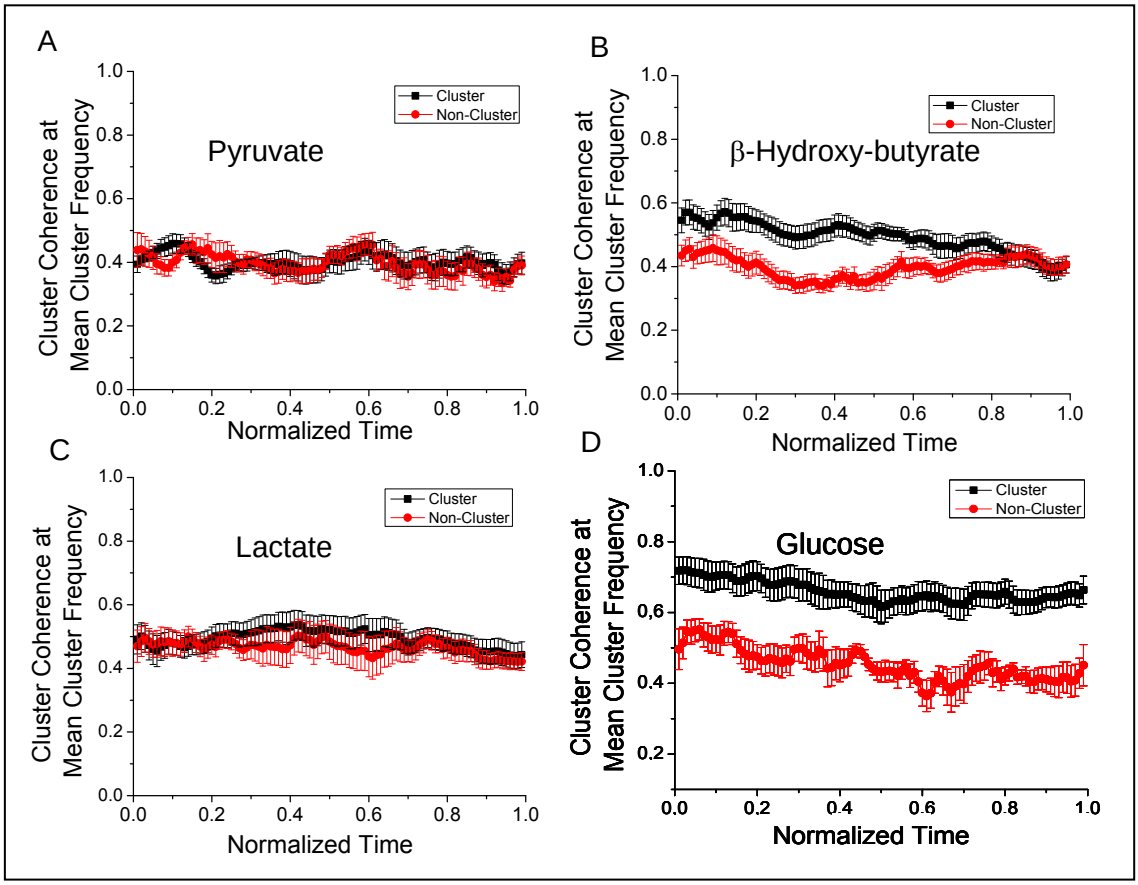

Figure S5 Coherence of mitochondria belonging to the major oscillating cluster, estimated at the mean cluster frequency, for 10mM of pyruvate (A; n=10), β-hydroxybutyrate (B; n=14), lactate (C; n=7), or glucose (D; n=9). To allow the statistical comparison between myocytes with unequal time recordings, the duration of the oscillations for each recording was normalized.

For each cluster mitochondrion, at each frequency, the average coherence in the running window was obtained from the average coherence over all nearest neighbors belonging to the cluster, followed by another averaging of the coherence over all cluster mitochondria. The fixed running window was subsequently shifted by one frame at a time until reaching the last frame of the recorded signal with its own last frame. A mean coherence for the mean major cluster frequency and for each running window was determined and plotted as a function of time. The length of recording for each myocytes was normalized to range from zero to one for a better comparison.

There was no significant change in the coherence of the cluster mitochondria during recording across the different substrate groups, indicating high temporal stability of the respective oscillating cluster mitochondria (Figure S5). However, the coherence of cluster mitochondria averaged in time seem to be highest in the glucose-treated cardiac myocytes being 0.66 ± 0.04, whereas the coherence in the pyruvate-, lactate- and β-hydroxybutyrate substrate groups were 0.40 ± 0.03, 0.49 ± 0.04 and 0.49 ± 0.03, respectively.

The coherence values for mitochondria that do not belong to the major cluster were estimated to be 0.44 ± 0.04, 0.39 ± 0.04, 0.46 ± 0.04 and 0.39 ± 0.03 for glucose-, pyruvate-, lactate- and β-hydroxybutyrate-treated cardiac myocytes, respectively. Thus, non-cluster mitochondria coherence appears to be high and similar across the different substrate groups. As suggested in (7) this may be due to stable oscillations of non-cluster mitochondria at frequencies that are different to the frequencies at which major cluster mitochondria oscillate. The coherence values observed for cluster and non-cluster mitochondria in glucose-treated myocytes (7) are consistent with those obtained in this work across all substrates, although less pronounced with lactate or pyruvate. This might be due to a decreased level of mitochondrial nearest-neighbor coupling during de- and repolarizations. Specifically, in the case of pyruvate-treated cardiomyocytes, smaller and more topologically dispersed ensembles of major cluster mitochondria have been observed. This increases the number of mitochondria within the major cluster that have at least one non-cluster nearest neighbor mitochondrion. Also, the number of non-cluster nearest neighbors for the majority of individual cluster mitochondria is increased. The alignment of temporal properties of a cluster mitochondrion with its neighboring mitochondria might therefore be less prominent, thus providing a lower averaged coherence.

Decay Rate Parameter γ

The γ value for each myocyte was optimized in the forward modeled whole myocyte TMRE signal to fit the experimental, amplitude-normalized TMRE fluorescent signal corresponding to the whole myocyte (Figures S6-S7). For each substrate, the mean decay rate parameter γ was quantified (in s^{-1}): $7.13 \cdot 10^{-2} \pm 1.55 \cdot 10^{-2}$ and $6.46 \cdot 10^{-2} \pm 1.14 \cdot 10^{-2}$ for glucose and β-hydroxybutyrate, respectively whereas pyruvate and lactate showed slightly smaller values: $6.10 \cdot 10^{-2} \pm 1.26 \cdot 10^{-2}$ and $6.29 \cdot 10^{-2} \pm 1.17 \cdot 10^{-2}$, respectively (Figure S7).

Forward Model and Model Validation

Forward modeling for whole-cell intensity signals with myocyte-specific γ and mitochondrial coupling constants was performed by cross-correlating the cosine of the whole-myocyte TMRE signal wavelet phase and the sum of cosines of the forward modeled phases of

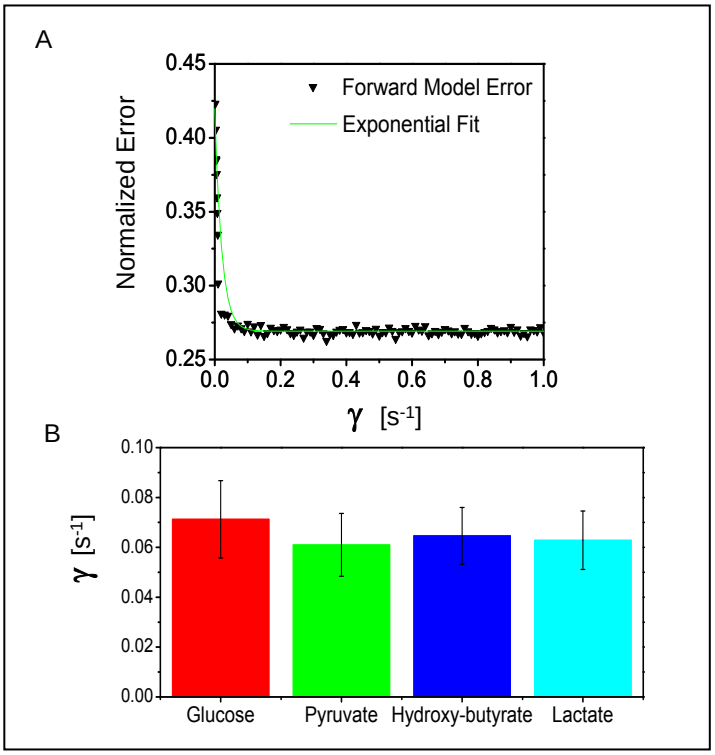

Figure S6 Minimum error estimation of decay rate parameter γ in the interval [0,1] s^{-1} for glucose, pyruvate, lactate and β-hydroxybutyrate respectively. (A) Normalized error of forward modeled γ-dependent stochastic phase model versus γ for a glucose-perfused cardiac myocyte. Exponential fit curve of type $f(x) = a \cdot \exp(-bx) + c$ (green line). Step increase of 0.01 s^{-1} starting from 0, the optimal decay rate parameter was chosen as the first γ whose error value was within 1% range of the value of the asymptotic error value (here, γ = 0.12 s^{-1}). (B) Values of the optimal decay rate parameters for glucose-, pyruvate-, β-hydroxybutyrate- and lactate-perfused cardiac myocytes. The γ distributions were not significantly different to each other (one-way ANOVA: F-value = 0.14, p-value = 0.9366).

the stochastic model (Figure S8). High correlation coefficients indicate the similarity of predicted and experimental signals, validating the determined coupling constants. Calculated correlation coefficients for each cardiac myocyte were 0.88 ± 0.02, 0.64 ± 0.05, 0.85 ± 0.03 and 0.75 ± 0.03 for glucose-, pyruvate-, lactate- and β-hydroxybutyrate-treated myocytes respectively (Figure S9).

The rather insignificant results for cardiac myocytes treated with pyruvate imply that the stochastic mitochondrial phase modeling may not be applicable when cardiac myocytes exhibit both a high degree of frequency dispersion and a low degree of cluster proximity. This problem could be partly avoided by only focusing on for example, ten cluster mitochondria that exhibit the highest averaged signal cross-correlation to their nearest neighbors thus ensuring cluster

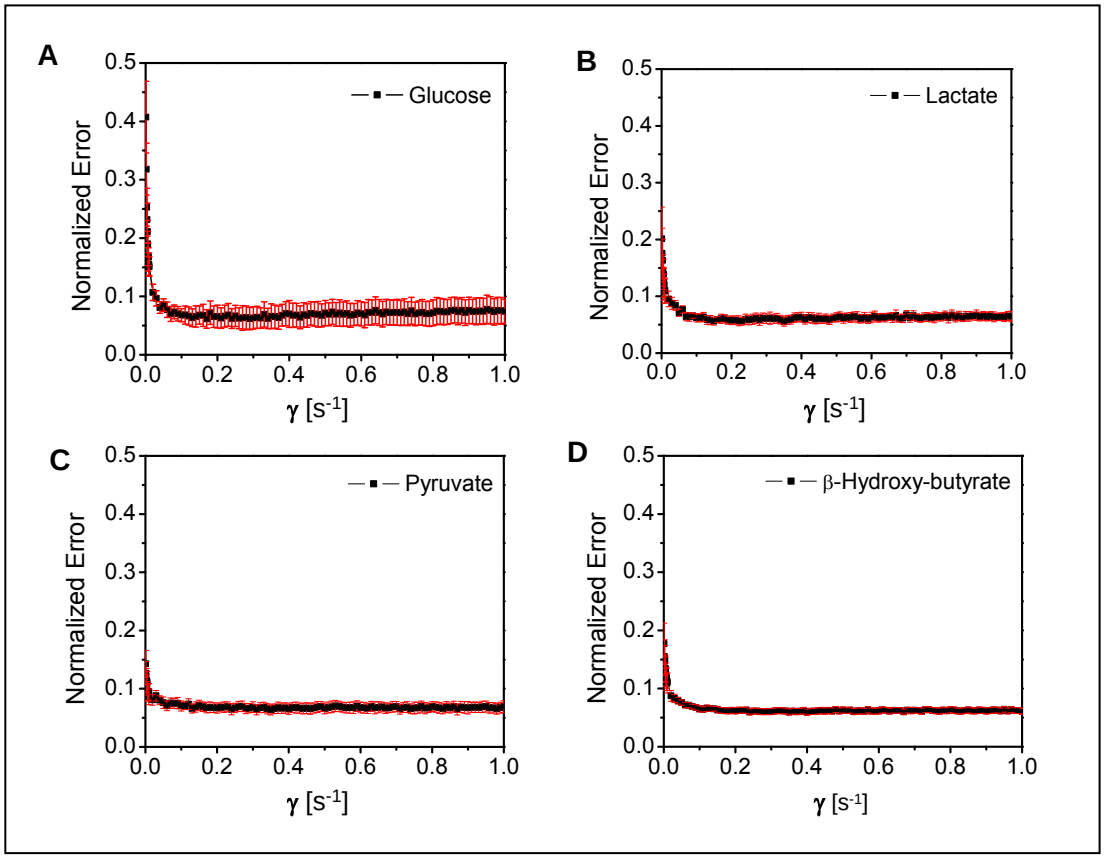

Figure S7 Normalized error versus decay rate parameter γ for all myocytes with perfusion in glucose (A; n=9), lactate (B; n=7), pyruvate (C; n=10), or β -hydroxybutyrate (D; n=14). Standard errors are displayed in red.

proximity. Subsequent cross-correlation of the cluster ensemble's individual cosine of the forward modeled phase signals with that of the cosine of the ensemble's wavelet phase, rendered high correlation coefficients 0.95 ± 0.02, 0.81 ± 0.04, 0.88 ± 0.05 and 0.86 ± 0.02 for glucose-, pyruvate-, lactate- and β-hydroxybutyrate-perfused myocytes, respectively (Figure S9).

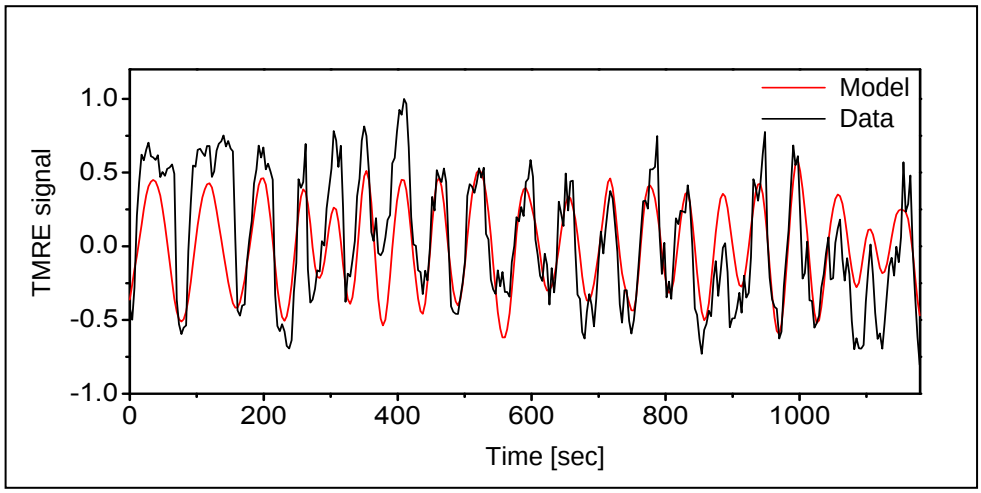

Figure S8 Forward modeling with optimal decay rate parameter γ and model validity. Normalized fluorescence intensity from experimental data for a lactate-perfused myocyte (black). The TMRE signal was subtracted the median value of the distribution, and the corresponding signal was normalized respect to its maximum value. Forward modeled cosine phase signals from all mitochondria (red line).

Spatio-temporal Properties of Local Coupling in Mitochondrial Frequency Clusters

To further explore effects of inter-mitochondrial coupling on network organization, mitochondrial mean cluster coupling constants were plotted versus % cluster area and mean cluster frequency for each point in time (Figures S10 and S11). As detailed above, time-dependent cluster affiliation for mitochondria had been determined according to dynamic mitochondrial frequency behavior and not morphological proximity. Therefore, a quantification of inter-mitochondrial coupling for local environments with nearest-neighbor-coupling was not considered to necessarily imply a link with temporal cluster organization. In this work, coupling is considered to be mediated by ROS via a diffusion-based process (1, 19, 20).

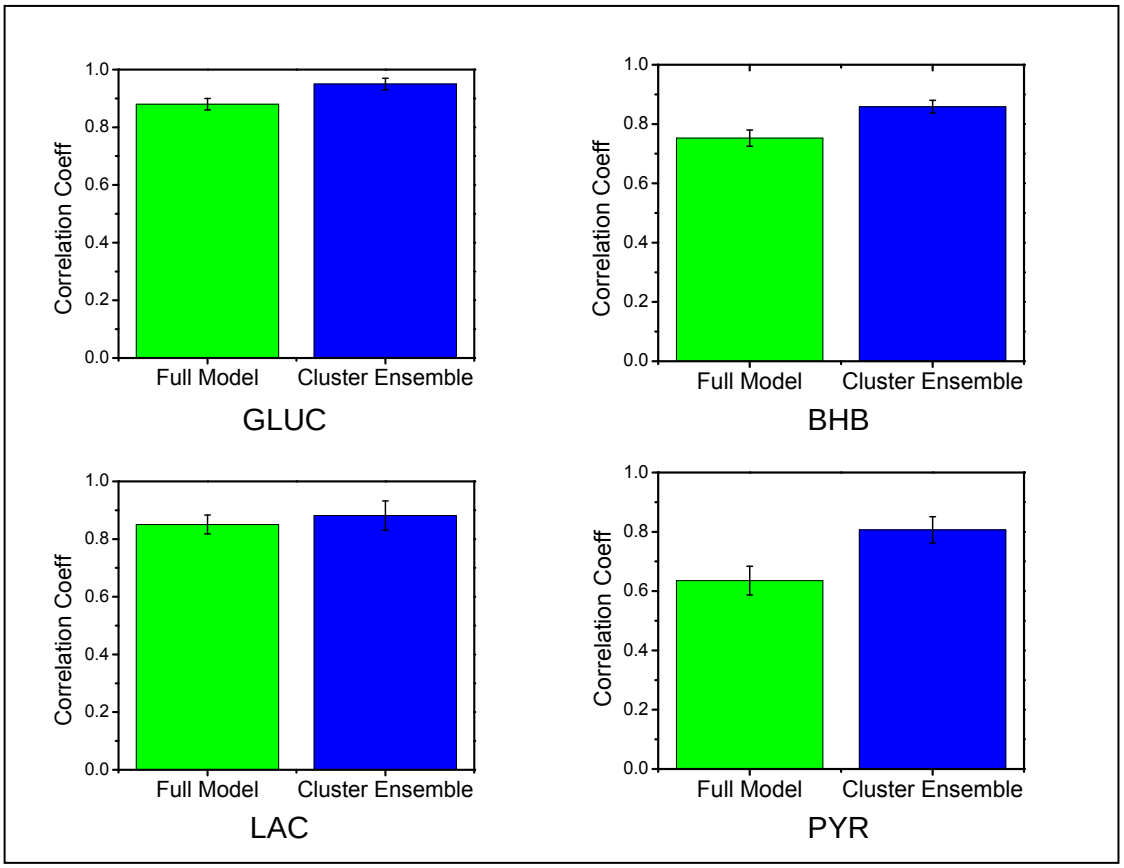

Figure S9 Cross-correlation coefficients for forward modeled signal to the cosine of the wavelet-determined phase of the whole myocyte signal (right hand side bar in each panel) in glucose (GLUC), β-hydroxy butyrate (BHB), lactate (LAC) or pyruvate (PYR). Smaller correlation coefficients in pyruvate-perfused cardiac myocytes reveal limitations of the stochastic mitochondrial phase model for cardiac myocytes with both a high degree of frequency dispersion and a low degree of cluster contiguity. Only considering the 10 cluster mitochondria with the highest averaged signal cross-correlation to their nearest neighbors (left hand side bar in each panel) yields satisfying correlation coefficients since cluster contiguity is most likely ensured.

Linear polynomial fitting yielded a slightly ascending linear function for cluster coupling (in s^{-1}) versus % cluster area with a slope of $2.04 \cdot 10^{-2} \pm 0.53 \cdot 10^{-2}$ s^{-1}/% for glucose-perfused myocytes (Figure S10). This tendency could be confirmed in myocytes perfused with lactate ($4.98 \cdot 10^{-2} \pm 0.30 \cdot 10^{-2}$ s^{-1}/%) or pyruvate ($4.63 \cdot 10^{-2} \pm 0.54 \cdot 10^{-2}$ s^{-1}/%). In these cases, inter-mitochondrial coupling grows with % cluster size indicating an overall increase in coupling strength for nearest-neighbor coupling leading to synchronization of the whole network. In contrast, β-hydroxybutyrate-perfused cardiac myocytes rendered a descending slope ($-4.70 \cdot 10^{-2}$

± $0.20 \cdot 10^{-2}$ s^{-1}/%). This difference as compared to the other substrates indicates altered organizational principles of the mitochondrial network that may be governed by metabolic effects of β–hydroxybutyrate on the ROS-induced ROS release mechanism.

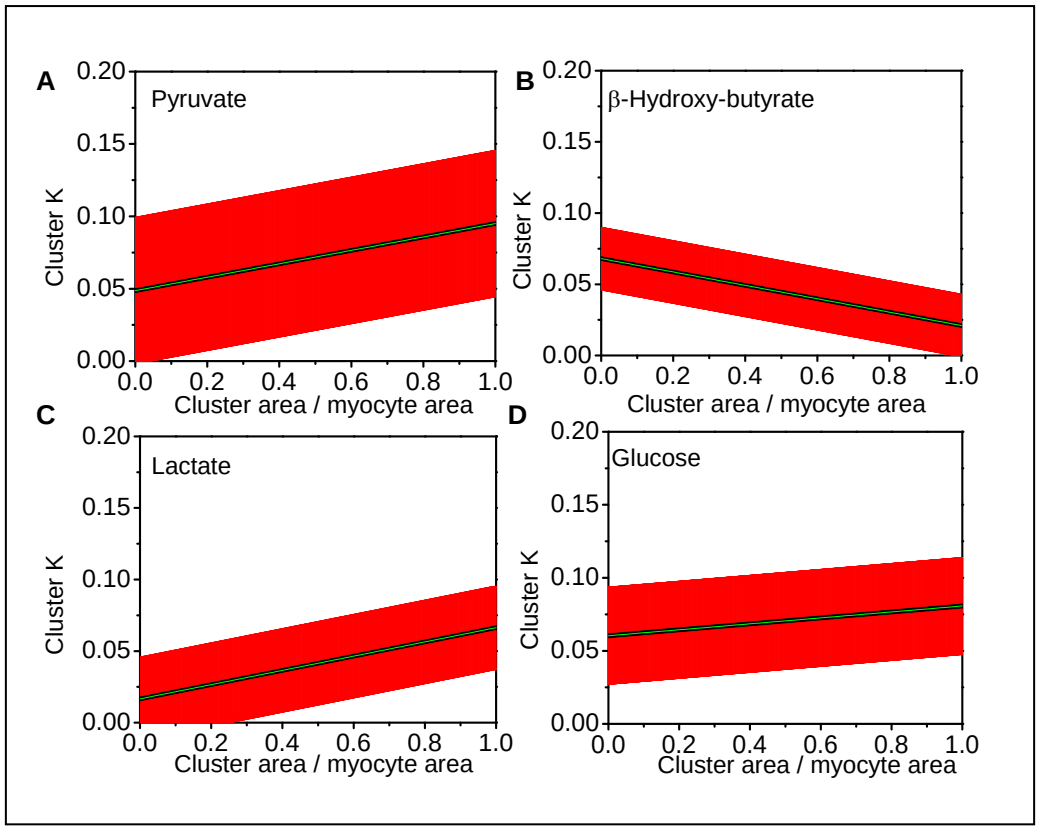

Figure S10 Linear fit with standard errors (red) of mean mitochondrial cluster constant (in s^{-1}) versus % cluster area for each point in time across all substrates, pyruvate (A), β-hydroxy-butyrate (B), lactate (C) or glucose (D). For glucose, pyruvate and lactate, inter-mitochondrial coupling grows with % cluster size, indicating an overall increase in coupling strength for nearest-neighbor coupling associated with synchronization of the whole network. However, β-hydroxybutyrate-perfused cardiac myocytes do not exhibit the same behavior indicating that cluster formation is influenced by additional redox or metabolic processes.

In contrast, linear regression on mitochondrial mean cluster coupling constants (in s^{-1}) versus mean mitochondrial cluster frequency (in mHz) gave a linear fit across the different substrates (Figure S11) with similar slopes of $3.31 \cdot 10^{-3} \pm 0.1 \cdot 10^{-3}$ $s^{-1}mHz^{-1}$, $3.14 \cdot 10^{-3} \pm 0.03 \cdot 10^{-3}$ $s^{-1}mHz^{-1}$, $4.01 \cdot 10^{-3} \pm 0.09 \cdot 10^{-3}$ $s^{-1}mHz^{-1}$ and $3.07 \cdot 10^{-3} \pm 0.04 \cdot 10^{-3}$ $s^{-1}mHz^{-1}$ for myocytes perfused with glucose, pyruvate, lactate and β-hydroxybutyrate, respectively. The results

indicate that the strength of local nearest-neighbor coupling is highest for cluster mitochondria oscillating at high frequency.

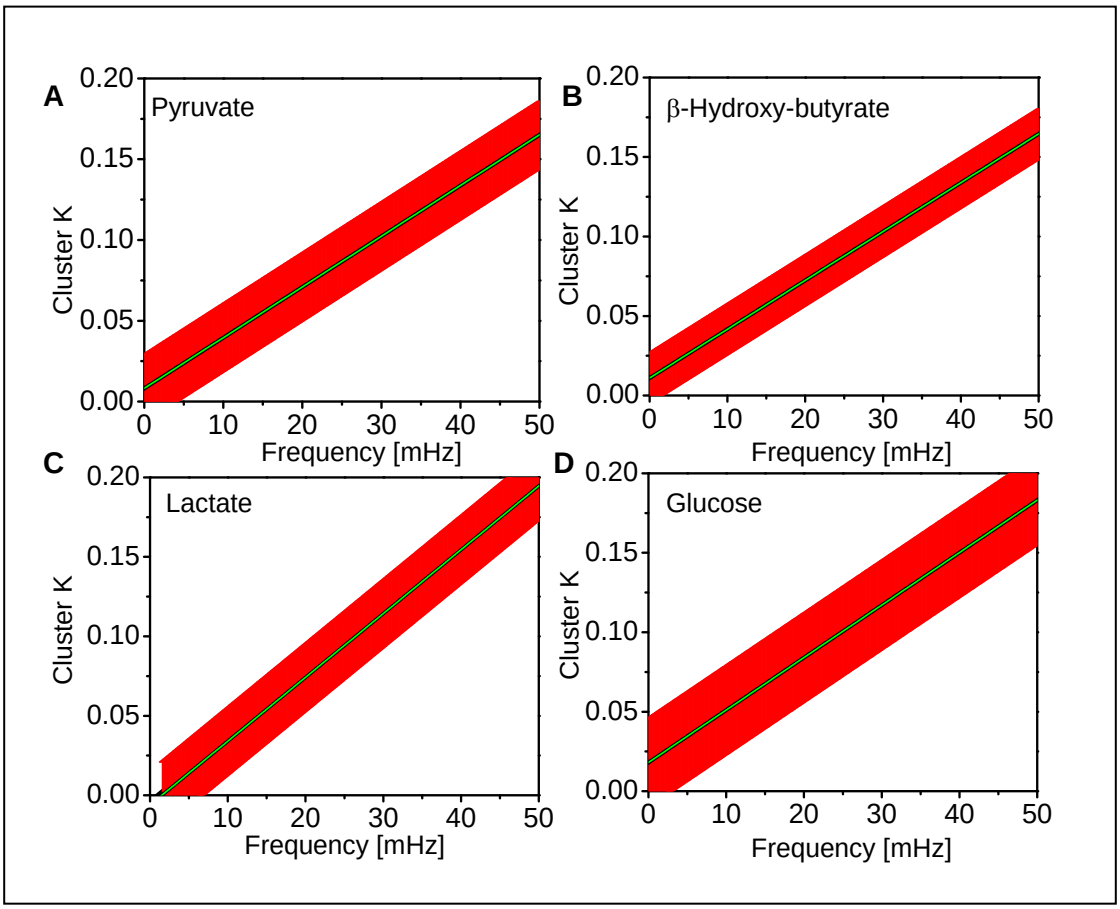

Figure S11 Linear fit with standard errors of mean mitochondrial cluster coupling constant (in s^{-1}) versus mean mitochondrial cluster frequency (in mHz) for each point in time and substrate pyruvate (A), β-hydroxy-butyrate (B), lactate (C) or glucose (D). In all substrates, higher frequencies are positively correlated with strong local nearest-neighbor coupling.

Figures Legends

Figure S1 Two-photon image of TMRE fluorescence from intact guinea pig heart tissue (different to the one shown in Figure 3 of the main text). (A) Within the intact heart tissue, cardiac myocytes were selected according to observed depolarizations. Myocyte borders along the sarcolemma and intercalated discs, as well as the mitochondrial grids were manually applied on a pixel-by-pixel basis. Yellow boxes mark the laser flashed region of the myocytes (see main text). Mitochondrial major cluster properties of the optical slice of perfused heart tissue shown in part A (n = 9 cardiac myocytes). Displayed are the mean cluster radius versus frequency (B); the cluster area normalized by the full myocyte area versus frequency (C); the distribution of mitochondrial frequencies for all cluster mitochondria across all myocytes (D), and the cluster mitochondria count normalized by the total number of mitochondria for the major cluster versus frequency (E). A similar figure for another optical slice of the intact heart tissue can be foud in the main text (Figure 1A and Figure 3).

Figure S2 Mitochondrial mean cluster radius as a function of frequency. Isolated cardiac myocytes were imaged as described in Methods and perfused as described in the legend of Figure 4 with 10mM of pyruvate(A; n=10), β-hydroxybutyrate (B; n=14), lactate (C; n=7), or glucose (D; n=9) .

Figure S3 Mitochondrial cluster count normalized by the total number of mitochondria for the major cluster versus frequency for isolated cardiac myocytes perfused with 10mM of pyruvate (A; n=10), β-hydroxybutyrate (B; n=14), lactate (C; n=7), or glucose (D; n=9) .

Figure S4 Distribution of mitochondrial frequencies for all cluster mitochondria across all myocytes perfused with 10mM of pyruvate (A; n=10), β-hydroxybutyrate (B; n=14), lactate (C; n=7), or glucose (D; n=9).

Figure S5 Coherence of mitochondria belonging to the major oscillating cluster, estimated at the mean cluster frequency, for 10mM of pyruvate (A; n=10), β-hydroxybutyrate (B; n=14), lactate (C; n=7), or glucose (D; n=9). To allow the statistical comparison between myocytes with unequal time recordings, the duration of the oscillations for each recording was normalized.

Figure S6 Minimum error estimation of decay rate parameter γ in the interval [0,1] s^{-1} for glucose, pyruvate, lactate and β-hydroxybutyrate respectively. (A) Normalized error of forward modeled γ-dependent stochastic phase model versus γ for a glucose-perfused cardiac myocyte. Exponential fit curve of type $f(x) = a \cdot \exp(-bx) + c$ (green line). Step increase of 0.01 s^{-1} starting from 0, the optimal decay rate parameter was chosen as the first γ whose error value was within 1% range of the value of the asymptotic error value (here, γ = 0.12 s^{-1}). (B) Values of the optimal decay rate parameters for glucose-, pyruvate-, β-hydroxybutyrate- and lactate-perfused cardiac myocytes. The γ distributions were not significantly different to each other (one-way ANOVA: F-value = 0.14, p-value = 0.9366).

Figure S7 Normalized error versus decay rate parameter γ for all myocytes with perfusion in glucose (A; n=9), lactate (B; n=7), pyruvate (C; n=10), or β -hydroxybutyrate (D; n=14). Standard errors are displayed in red.

Figure S8 Forward modeling with optimal decay rate parameter γ and model validity. Normalized fluorescence intensity from experimental data for a lactate-perfused myocyte (black). The TMRE signal was subtracted the median value of the distribution, and the corresponding signal was normalized respect to its maximum value. Forward modeled cosine phase signals from all mitochondria (red line).

Figure S9 Cross-correlation coefficients for forward modeled signal to the cosine of the wavelet-determined phase of the whole myocyte signal (right hand side bar in each panel) in glucose (GLUC), β-hydroxy butyrate (BHB), lactate (LAC) or pyruvate (PYR). Smaller correlation coefficients in pyruvate-perfused cardiac myocytes reveal limitations of the stochastic mitochondrial phase model for cardiac myocytes with both a high degree of frequency dispersion and a low degree of cluster contiguity. Only considering the 10 cluster mitochondria with the highest averaged signal cross-correlation to their nearest neighbors (left hand side bar in each panel) yields satisfying correlation coefficients since cluster contiguity is most likely ensured.

Figure S10 Linear fit with standard errors (red) of mean mitochondrial cluster constant (in s^{-1}) versus % cluster area for each point in time across all substrates, pyruvate (A), β-hydroxy-

butyrate (B), lactate (C) or glucose (D). For glucose, pyruvate and lactate, inter-mitochondrial coupling grows with % cluster size, indicating an overall increase in coupling strength for nearest-neighbor coupling associated with synchronization of the whole network. However, β-hydroxybutyrate-perfused cardiac myocytes do not exhibit the same behavior indicating that cluster formation is influenced by additional redox or metabolic processes.

Figure S11 Linear fit with standard errors of mean mitochondrial cluster coupling constant (in s^{-1}) versus mean mitochondrial cluster frequency (in mHz) for each point in time and substrate pyruvate (A), β-hydroxy-butyrate (B), lactate (C) or glucose (D). In all substrates, higher frequencies are positively correlated with strong local nearest-neighbor coupling.

Table Captions

Table S1 Stochastic phase model with drifting frequencies and time-dependent local mitochondrial coupling. (A) An extended Kuramoto model for the oscillator phases $\varphi_m(t)$ and frequencies $\omega_m(t)$ describes coupled circadian phase oscillators. N_m is the total number of nearest neighbors of mitochondrion m. The sum of the coupling term runs over all nearest neighbors j_m of mitochondrion m. The total luminescence signal $s(t)$ is the sum of a population of all oscillators contributing an amplitude-normalized cosine signal. M is the total number of mitochondrial oscillators and the sum of cosines runs over all mitochondrial oscillators. (B) Parameter listing. $K_m(t)$ represents the time-dependent local mitochondrial phase coupling constant.

Table S2 Multi-Peak Gaussian fit analysis for peaks in the frequency distributions of cardiac myocytes perfused with different substrates. For each peak, the mean frequency ± the FWHM are given in mHz.

Supporting References

1. Aon, M. A., S. Cortassa and B. O'Rourke. 2006. The fundamental organization of cardiac mitochondria as a network of coupled oscillators. Biophys. J. 91: 4317-4327.

2. Aon, M. A., S. Cortassa, E. Marban and B. O'Rourke. 2003. Synchronized whole cell oscillations in mitochondrial metabolism triggered by a local release of reactive oxygen species in cardiac myocytes. J. Biol. Chem. 278: 44735-44744.

3. O'Rourke, B. R., B.M. and E. Marban. 1994. Oscillations of Membrane Current and Excitability Driven by Metabolic Oscillations in Heart Cells. Science. 265: 962–966.

4. Backx, P. H., W. D. Gao, M. D. Azan-Backx and E. Marban. 1994. Mechanism of force inhibition by 2,3-butanedione monoxime in rat cardiac muscle: roles of [Ca2+]i and cross-bridge kinetics. J. Physiol. 476: 487-500.

5. Slodzinski, M. K., M. A. Aon and B. O'Rourke. 2008. Glutathione oxidation as a trigger of mitochondrial depolarization and oscillation in intact hearts. J. Mol. Cell. Cardiol. 45: 650-660.

6. Kurz, F. T., M. A. Aon, B. O'Rourke and A. A. Armoundas. 2010. Wavelet analysis reveals heterogeneous time-dependent oscillations of individual mitochondria. Am. J. Physiol. Heart Circ. Physiol. 299: H1736-1740.

7. Kurz, F. T., M. A. Aon, B. O'Rourke and A. A. Armoundas. 2010. Spatio-temporal oscillations of individual mitochondria in cardiac myocytes reveal modulation of synchronized mitochondrial clusters. Proc. Natl. Acad. Sci. USA. 107: 14315-14320.

8. Garcia-Ojalvo, J., M. B. Elowitz and S. H. Strogatz. 2004. Modeling a synthetic multicellular clock: repressilators coupled by quorum sensing. Proc. Natl. Acad. Sci. USA. 101: 10955-10960.

9. Rougemont, J. and F. Naef. 2007. Dynamical signatures of cellular fluctuations and oscillator stability in peripheral circadian clocks. Mol. Syst. Biol. 3: 93.

10. Suel, G. M., J. Garcia-Ojalvo, L. M. Liberman and M. B. Elowitz. 2006. An excitable gene regulatory circuit induces transient cellular differentiation. Nature. 440: 545-550.

11. Rougemont, J. and F. Naef. 2006. Collective synchronization in populations of globally coupled phase oscillators with drifting frequencies. Phys. Rev. E 73: 011104.

12. Lemons, D. 2002. An Introduction to Stochastic Processes in Physics. The Johns Hopkins University Press. Baltimore and London.

13. Hong, H. and S. H. Strogatz. 2011. Kuramoto model of coupled oscillators with positive and negative coupling parameters: an example of conformist and contrarian oscillators. Phys. Rev. Lett. 106: 054102.

14. Kuramoto, Y. 1984. Chemical oscillations, waves, and turbulence. Springer-Verlag.

. Berlin.

15. O'Leary, D. P. 2001. Near-optimal parameters for Tikhonov and other regularization methods. SIAM J. Sci. Comput. 23: 1161 - 1171.

16. Park, H. W., S. Shin and H. S. Lee. 2001. Determination of an optimal regularization factor in system identification with Tikhonov regularization for linear elastic continua. Int. J. Numer. Meth. Eng. 51: 1211-1230.

17. Aon, M. A., S. Cortassa, F. G. Akar and B. O'Rourke. 2006. Mitochondrial criticality: a new concept at the turning point of life or death. Biochim. Biophys. Acta. 1762: 232-240.

18. Aon, M. A., S. Cortassa and B. O'Rourke. 2004. Percolation and criticality in a mitochondrial network. Proc. Natl. Acad. Sci. USA. 101: 4447-4452.

19. Zhou, L., M. A. Aon, T. Almas, S. Cortassa, R. L. Winslow and B. O'Rourke. 2010. A Reaction-Diffusion Model of ROS-Induced ROS Release in a Mitochondrial Network. PLoS Comput. Biol. 6: e1000657.

20. Fang, H., M. Chen, Y. Ding, W. Shang, J. Xu, X. Zhang, W. Zhang, K. Li, Y. Xiao, F. Gao, S. Shang, J.-C. Li, X.-L. Tian, S.-Q. Wang, J. Zhou, N. Weisleder, J. Ma, K. Ouyang, J. Chen, X. Wang, M. Zheng, W. Wang, X. Zhang and H. Cheng. 2011. Imaging superoxide flash and metabolism-coupled mitochondrial permeability transition in living animals. Cell Res. 21: 1295-1304.